communications earth & environment

ARTICLE

https://doi.org/10.1038/s43247-022-00633-0 OPEN

Asian monsoon intensity coupled to Antarctic climate during Dansgaard–Oeschger 8 and Heinrich 4 glacial intervals

Yi-Jia Liang[1,2], Shi-Tao Chen[2✉], Yong-Jin Wang[2], Kan Zhao[2], Shao-Hua Yang[3], Zhen-Jun Wang[2], Yu-Zheng Huang[2], Hai Cheng[4] & R. Lawrence Edwards[2,5]

The transition from glacial to interglacial periods has been hypothesized to be linked to millennial-scale changes in oceanic/atmospheric circulation, but the relationships between these phenomena remain poorly constrained. Here we present a speleothem oxygen isotope record from Yongxing Cave, China, spanning 40.9 to 33.1 ka and compare this to existing Antarctic proxy records. We find that decadal-to-centennial rapid shifts in the Asian summer monsoon, Antarctic temperature, atmospheric methane and carbon dioxide are all coupled together during Dansgaard–Oeschger cycles, which may suggest an important role of the Intertropical Convergence Zone and Southern Ocean in driving the global greenhouse gas changes. Analogous to millennial-scale variations in trend, amplitude and internal sub-centennial-scale structures during Dansgaard–Oeschger 8 and Heinrich Stadial 4, the Younger Dryas and Heinrich Stadial 1 during the last ice termination provided critical positive feedbacks to changes in terrestrial vegetation and northern ice volume, and may have contributed to glacial to interglacial transition.

[1] School of Geographic Science, Nantong University, Nantong 226007, China. [2] School of Geography, Nanjing Normal University, Nanjing 210023, China. [3] College of Economy and Management, Nanjing Vocational University of Industry Technology, Nanjing 210023, China. [4] Institute of Global Environmental Change, Xi'an Jiaotong University, Xi'an 710054, China. [5] Department of Earth and Environmental Sciences, University of Minnesota, Minneapolis, MN 55455, USA. ✉email: chenshitao@njnu.edu.cn

During the last ice age, the well-known millennial-scale events, including the Dansgaard–Oeschger (DO) cycles and Heinrich Stadial (HS) in the North Atlantic, and the Antarctic Isotopic Maxima (AIM) events in the Antarctica[1–5], are anti-phased related, and likely driven by changes in the intensity of the Atlantic Meridional Overturning Circulation (AMOC), as conceptualized in the bipolar seesaw mechanism[6]. However, their characteristics and mechanisms remain in hot debate, including the apparent hemispheric asymmetry characteristic of DO-AIM events[4,7], uncertain lead-lag relationships of the Northern Hemisphere (NH) and Southern Hemisphere (SH)[5], external forcing of volcanism and solar activities[8,9], roles of oceanic/atmospheric circulations in transferring the climatic signals[10,11], etc. With the emergence of high-resolution geological records, detailed characteristics in the Greenland ice cores are found distinctive from records in the Antarctica and other regions. Few counterparts and abrupt changes in the Greenland ice cores could be found in archives from the Antarctica and other regions[7,12], indicating that Greenland-type changes are regional while the Antarctic-type variability is likely of global significance[13,14]. Furthermore, fast shifts in greenhouse gases (CH_4 and CO_2) within millennial-scale HS events are observed, indicating mechanisms involving centennial-scale oscillations in regulating millennial climates[15–17]. Although those millennial-scale changes that occurred across the last ice terminations (T1) were extensively regarded as important forcings[18–20], a further investigation on nature and mechanism of millennial-scale change will help to understand mechanisms behind the glacial-interglacial transition.

The analogs of the millennial-scale changes between different glacial-interglacial cycles provide critical constraints on their mechanisms. Similar frequency and amplitude of millennial events between the penultimate and the last glacial period have been observed, suggestive of an importance of orbital control[21,22]. Furthermore, throughout the Late Pleistocene, analogous nature and structures of millennial-scale monsoonal events across the last four terminations[23] and mega-weak monsoon intervals associated with each termination[18] indicate that the millennial-scale events are likely the pacemakers for the transition from glacial to interglacial periods. During the last glacial period, temperature changes in the AIM events are proportional with Antarctic termination during the first 1500 years, hence the southern warming is supposed to be an initial trigger for the terminations[24]. Previous study compared the intensity of ocean circulation in the SH during the last 40 ka and highlighted the importance of vigorous circulation in triggering T1[25]. This point of view is further supported by ref. [26]. Changing sequences of ice sheets in the New Zealand and the Asian summer monsoon similar to that of the T1 were found at the transition of Marine Isotope Stage 4/3 (MIS4/3t), namely the unfinished termination[18,27,28]. These studies display the strong self-similarity and possible recurrences of the Earth's climate system, although analogs in ancient climates were not that perfect.

Asian Monsoon changes, as revealed by radiometric-dated cave speleothems, are characterized by a typical pattern of precessional cycles which follow changes in NH insolation[18,21]. Superimposed on the long-term insolation changes are series of millennial signals which can be related to both climate changes at the Greenland and the Antarctica[28–32]. A dominant SH control on millennial-scale monsoon variability was found documented in Hulu stalagmites during glacial times and a NH control during deglacial and interglacial times[32]. Hence, millennial-scale monsoon changes on the precessional climate background provide a potential to reveal an analog between different precessional cycles, which assists understanding of the millennial-scale oscillations and the glacial-interglacial theory.

Here we present data from Yongxing Cave, China, to demonstrate an analogous feature of millennial-scale changes during the last glacial period. Previous publications from Yongxing Cave, including detailed information on the DO-AIM events imprinted on East Asian summer monsoon (EASM)[30], decadal-to-centennial-scale changes during the last interglacial[33] and annually-resolved data across the MIS11[34], highlight that speleothem records from this cave are optimal to reconstruct high-resolution Asian monsoon changes. More importantly, our record has comparable counterparts with those in Antarctic/Greenland ice core records on the millennial to sub-centennial timescales, indicating a global feature imprinted in the monsoon changes. Further comparison of climatic sequences on the rising limbs of the NH insolation indicates recurrences of the millennial-scale events in transitions on different timescales.

Results and discussion

Reconstructed YX $\delta^{18}O$ record and its climatic interpretation. We determined 9 dates using ^{230}Th dating techniques and established the chronologies of all samples by using an objective age model algorithm (see Supporting Materials and Methods, Fig. S1); and in total, we measured 826 stable isotopic values. Our high-resolution record then covers the latter part of the Marine Isotope Stage (MIS) 3, including DO events 6 to 9 and HS4 as found in Greenland ice cores (Fig. 1; Supplementary Data 1). During the entire growth interval, the average of $\delta^{18}O_{calcite}$ values is −8.6‰, featured with a relatively positive-valued period from 39.8 to 38.1 ka BP that outstands the whole record. $\delta^{18}O_{calcite}$ record has a 4‰ range from −10.1‰ to −6.1‰, superimposed by large-amplitude millennial-scale fluctuations and sub-millennial-scale oscillations, strikingly similar to other speleothem records from the same cave and other caves in Southern China (Fig. S2). This indicates that speleothem $\delta^{18}O_{calcite}$ is consistent with insignificant kinetic fractionation[35] in Yongxing Cave. Although we have only 9 dating results, HS4 event could be well-constrained. Compared with most of the previously-published records (Fig. S2), our record has a long and continuous temporal coverage, high resolution and good dating constraints, displaying good potential in investigating climatic dynamics.

We here regard the speleothem $\delta^{18}O_{calcite}$ as a proxy of the EASM intensity following several lines of reasoning. Firstly, a 3-year monitoring work in Yongxing Cave shows that cave dripwater and modern speleothem calcite mainly inherit $\delta^{18}O$ signals in precipitation, especially the wet-season recharge from May to September[36] when ~70% of the annual precipitation is received (Fig. S3a). Correlation between the amount-weighted annually-averaged precipitation $\delta^{18}O$ and the annual summer rainfall ratio at the study site reaches 0.37 ($n = 38$, $p < 0.01$) (Fig. S3b), also indicating that $\delta^{18}O$ at the cave site is modulated by the EASM-related rainfall. Secondly, comparison of the YX92 $\delta^{18}O$ record[37] from the same cave with historical flood/drought index series reconstructed in the Yangtze River Valley[38] as well as the long-term EASM index record[39] shows good correspondence and correlations during the overlapped interval extending back to 1785 AD, with lighter $\delta^{18}O$ consistent with more flood events and higher EASM index (strong monsoon), and vice versa (Fig. S4). In sum, from the view of modern climatology, speleothem $\delta^{18}O$ is controlled by summer monsoon rainfall $\delta^{18}O$ to a large extent[36]. Furthermore, both geochemical proxies and petrographic analyses of YX55 sample from the same cave, which grew during 65 and 40 ka BP, provide strong evidence that positive shifts in calcite $\delta^{18}O$ correlate to dry conditions controlled by weak monsoon[40]. It is found that during HS intervals, the deposition rate of

stalagmite was relatively low, along with strong prior calcite precipitation processes (indicated by high trace metal ratios), and the corresponding lithological section is composed of dense and fibrous minerals; these features are opposite from those during the DO Interstadials[40]. Besides, our previous review[41] on the cave records in Asia and modeling shows that two mechanisms affect stalagmite $\delta^{18}O$: changes in the fraction of monsoon rainfall in annual totals and changes in the amount of rainout between tropical sources and cave sites. The former is caused by changes in the seasonal migration of the sub-tropical jet and the dominant latter one involves changes in rainout from both the Pacific and the Indian Ocean sources. Therefore, we suggest that speleothem $\delta^{18}O$ represents the EASM intensity and the related precipitation, as suggested in previous studies[18,21,23,41].

Coupling of monsoon and Antarctic climates. The structure of YX $\delta^{18}O_{calcite}$ record depicts a variability that captures both Greenland and Antarctic climate signals (Fig. 1), and the millennial-scale relationship has been reported[30]. The structure of HS4 (AIM8) event is taken as an example here (Fig. 2) because both of its onset and ending are constrained by two ^{230}Th dates. We used the Rampfit method[42] to determine the inflections of HS4 transitions (red points in Fig. 2c). The fast 60-year enrichment centering around 39.9 ka BP and the abrupt negative jump around 38.2 ka in our cave record (both $\delta^{18}O$ shifts >1‰) can be aligned to the rapid decadal-scale cooling and warming of HS4 in NGRIP $\delta^{18}O_{ice}$ record. However, these rapid shifts in the $\delta^{18}O_{calcite}$ reached only half of the entire amplitude in the processes (Fig. 2a, b). In contrast, changes in the EASM intensity mimic the "trapezoid-shaped" Antarctic temperature profiles (Fig. 2g). At the onset of HS4, a gradually positive shift in $\delta^{18}O_{calcite}$ sustained until 39.5 ka BP, alike the gradual warming in Antarctica which lasted for ~500 years[7]. Within the HS4, the EASM was weak though, it was recovering at a slow pace, exceeding 1/3 the intensity of the Interstadial 8 onset (Fig. 2c). This precursor recovery supports the finding[43] that a CH_4 response in boreal wetland regions precedes the rapid onset of DO8. The weakening and recovery processes of the EASM can also be supported by consistent changes in Ca^{2+} concentration (Fig. 2b), which are tightly related to monsoon intensity via the jet stream[44]. Meanwhile, Antarctica warmed up at a slower rate (Fig. 2f), entering the second warming phase[7]. In detail, several centennial-scale changes between monsoon weakening and Antarctic warming are correlated within this stage. At the end of HS4, monsoon experienced twofold intensification around 38.2 ka BP, with a fast process at first (<60 years, $\delta^{18}O$ shift >1‰) and a much gradual interval lasting for ~240 years (Fig. 2c). The Antarctic temperature came to a "breakpoint" after the 1700-year warming, as described in ref. [7] (Fig. 2f). The onset of Interstadials in both NGRIP and YX records can be aligned to the "breakpoint" of the Antarctic AIM events[7], even if we take the 200-year lead of the Greenland into account[5]. The similar detailed changes in the $\delta^{18}O_{calcite}$ are also evidenced by the extensive cave records such as Hulu, Zhangjia, Xianyun and Mawmluh in Asian monsoon domain (Fig. S2). The structures in speleothem records are also captured by the NEEM ^{17}O excess data[45] representing low-latitude hydroclimate changes (Fig. 2d).

In general, our monsoon record exhibits the same duration, pattern and relative magnitude as the Antarctic record from AIM6 to AIM8 (Fig. 1), and the "trapezoid-shape" structure of HS4 (AIM8) is also recognized in AIM events 6 and 7 in YX record (Fig. 3), indicating that even a weak AIM can affect the EASM to some extent. Besides, YX record reproduces the Antarctic temperature variations on finer timescales, featured by the striking similarity at around 33.4, 33.7, 34.9, 35.7, 36.1, 38, and 39.9 ka BP on the speleothem chronology (yellows bars in Fig. 3). This finding could shed light on a close dynamic teleconnection between the SH oceanic-atmospheric dynamics

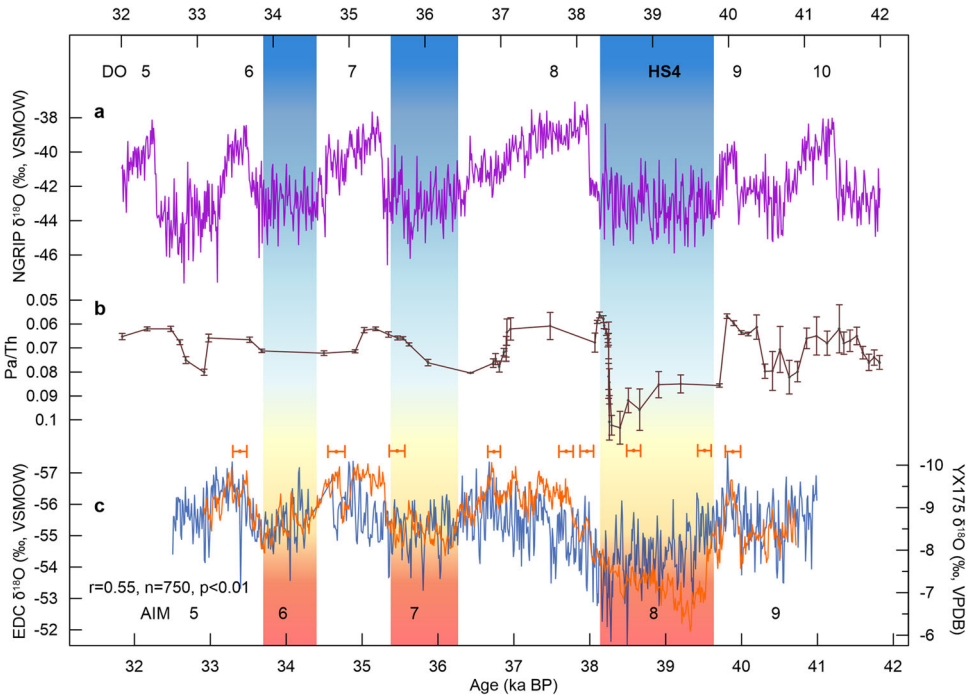

Fig. 1 Climate indices from 42 to 32 ka BP during the MIS3. a $\delta^{18}O_{ice}$ record from NGRIP ice core on the GICC05 chronology (purple)[1,86]. **b** Pa/Th ratios and error bars (SD) from the North Atlantic, indicating the AMOC strength (brown)[62]. **c** Our $\delta^{18}O_{calcite}$ record (orange) overlapped with $\delta^{18}O_{ice}$ record from the Antarctic EDC ice core on the AICC2012 chronology (blue)[7,87]. Numbers indicate DO events, AIM events and HS4. Orange dots indicating ^{230}Th dating results and SD errors. Pearson correlation coefficient is calculated between our $\delta^{18}O_{calcite}$ and EDC $\delta^{18}O$ record, denoted on the bottom-left corner.

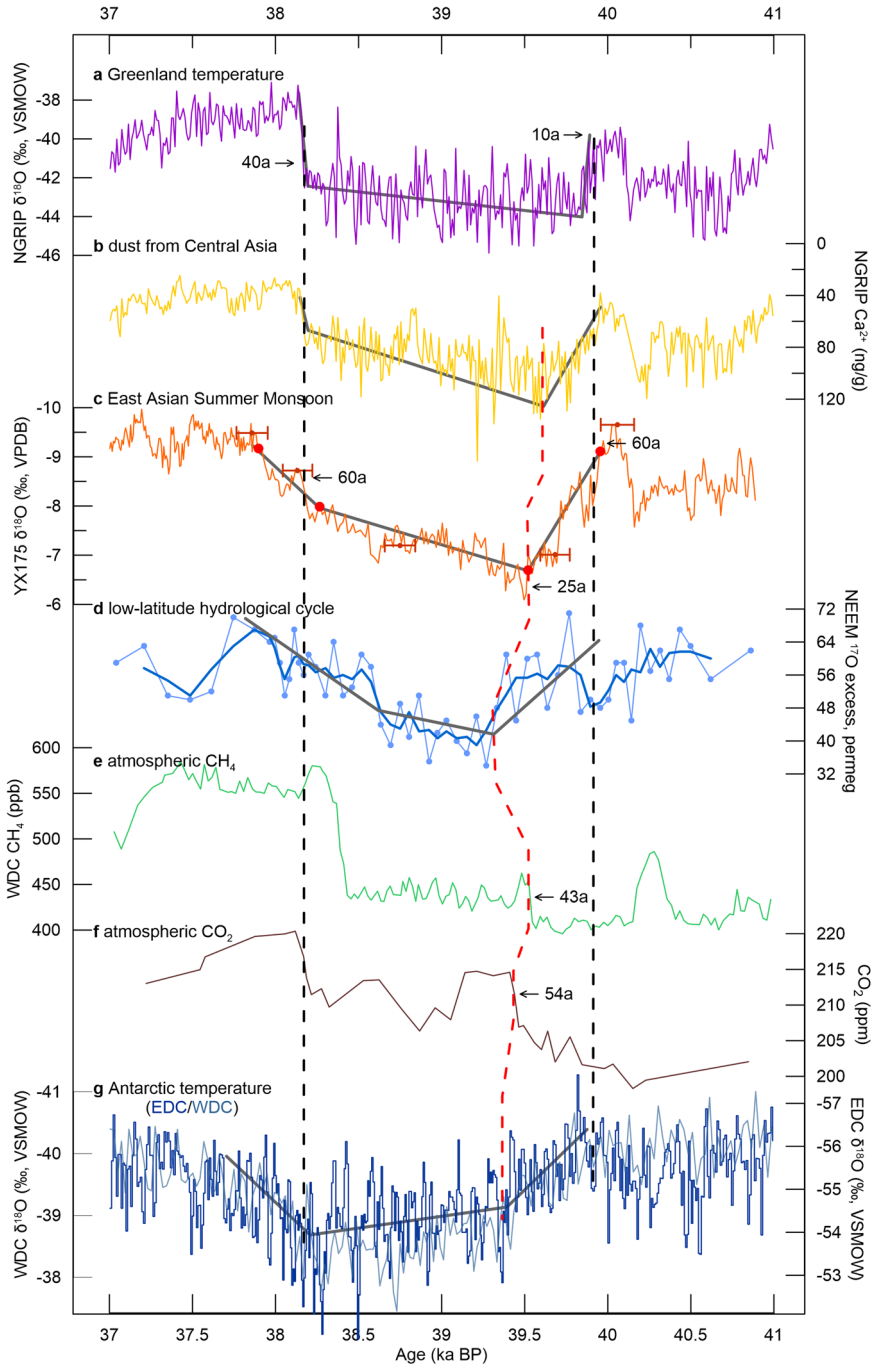

Fig. 2 Detailed view of the HS4 (AIM8) Structure. a $\delta^{18}O_{ice}$ (purple)[1] and **b** dust Ca^{2+} (yellow)[44] records from NGRIP ice core on the GICC05 chronology[86]. **c** YX175 $\delta^{18}O_{calcite}$ record and dating results with errors (orange). **d** NEEM ^{17}O-excess record (blue line and dots)[45]. **e** CH_4 records from WDC ice core on the WD2014 (green)[5,51]. **f** CO_2 record from Siple Dome (brown)[74]. **g** $\delta^{18}O_{ice}$ records from EDC ice core (navy blue)[7] on the AICC2012 chronology[87] and WDC ice core[5] (light blue) on the WD2014 chronology[51]. Black dashed lines indicate the onset and the end of the HS4 in NGRIP $\delta^{18}O_{ice}$ record, and the red one indicates the abrupt shifts in proxies. Five bold black polylines depict the structure of HS4 (AIM8). Phase division in Antarctic records in **f** follows[7]. Duration of rapid shifts in proxies are denoted.

and the NH monsoon intensities on different timescales. The Intertropical Convergence Zone (ITCZ), with the northerly ITCZ corresponding to the stronger monsoon status[46], is prone to move towards the warmer hemisphere in response to changes in cross-equatorial temperature gradients[47] caused by the AMOC intensity[48,49] as well as the Southern Ocean temperature[50]. During Stadials, Antarctic warming is coherent with temperature increase over the SH, thus leading to a southerly shift of the ITCZ and the weakening EASM. Besides, large amounts of moisture and latent heat export into inland China from the remote South Indian Ocean rely on the cross-equatorial airflow between the Mascarene High in the South Indian Ocean and low-pressure system over the Asian continent[51]. The cross-equatorial airflow carries 87% of the latent heat from the South Indian Ocean into the Indian sub-continent[52], and further northward into southern China, as a primary moisture source (53%) for summer precipitation at Yongxing site (Fig. S5). Being the most dominant extratropical annular mode in the SH, the Antarctic Oscillation

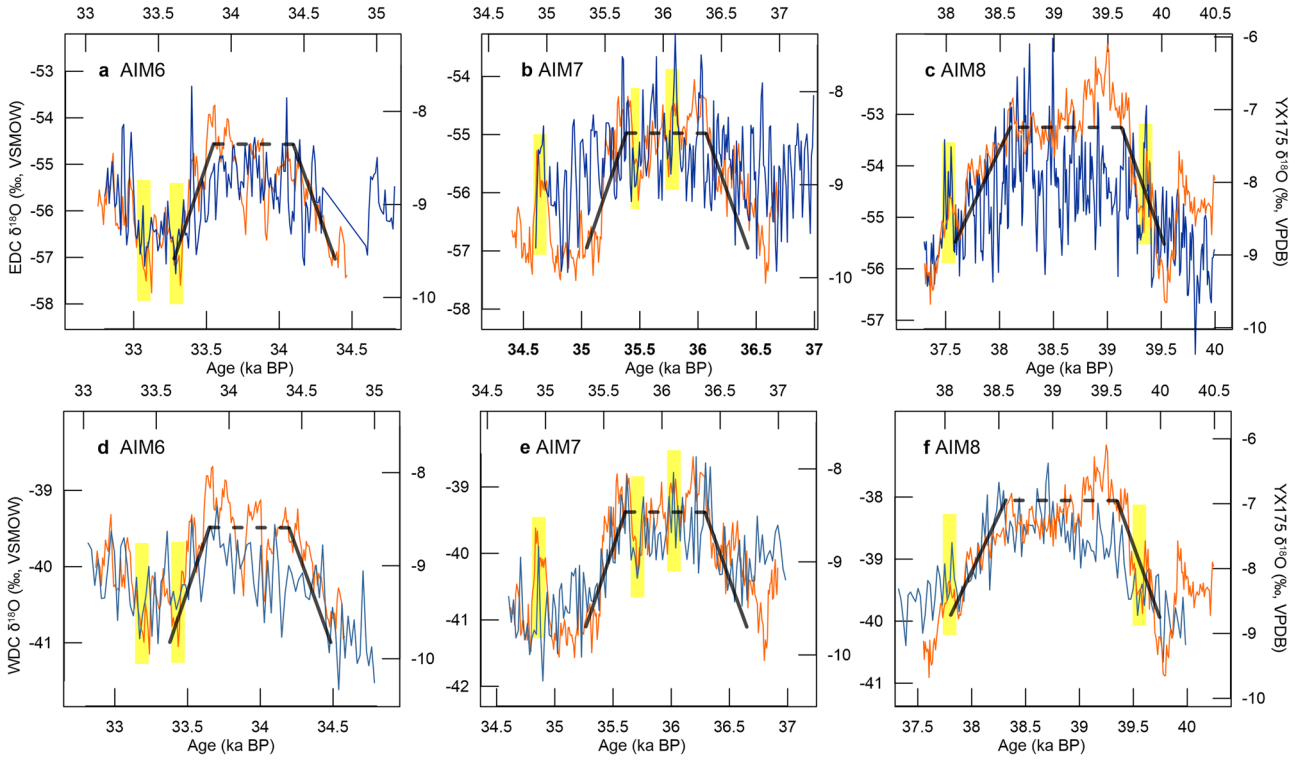

Fig. 3 The "Trapezoid-style" EASM changes during the AIM events. We aligned the weak monsoon events in YX (orange lines) and AIM events (including AIM6, AIM7 and AIM8 events) in the EDC $\delta^{18}O_{ice}$ (**a**–**c**) and WDC $\delta^{18}O_{ice}$ (**d**–**f**) records (blue lines). The comparison is within the AICC2012/WD2014 chronology's uncertainties, 500~900 years for AICC2012 and 350~400 years for WD2014[5,7,51,87]. Strong positive Pearson correlation coefficients are found of YX with EDC record ($r = 0.55$, $n = 750$, $p < 0.01$, Fig. 1c, with the EDC record tuned older by 340 years), and with WDC record ($r = 0.74$, $n = 788$, $p < 0.01$, Fig. 1c, with the WDC record tuned older by 200 years). Yellow bars indicate centennial to sub-centennial fluctuations in three records.

(AAO) controls the interannual variability of the Mascarene High[53]. The AAO involves a seesaw pattern between the pressure levels in the SH midlatitude and polar regions; and a positive AAO is characterised with low-pressure anomalies over the south pole and high-pressure anomalies over middle latitudes[54]. There are strong correlations between the AAO, the Mascarene High and the EASM[53,54]. Generally, a positive AAO in boreal spring is correlated with temperature increases in Antarctica and an intensification in the Mascarene High during boreal spring through summer, which is followed by a weakened EASM[53,54]. This seasonal sense of AAO variability could be extrapolated to the Antarctic Centennial Oscillation (ACO) which is a paleoclimate precursor of the contemporary AAO[55]. Were it so, the atmospheric propagation from the SH could cause similar variations in our EASM record even on the centennial timescales, operating in a way similar to the present day.

Despite a confounding effect of the two polar climates on the EASM pattern, the SH climates could shape tropical hydroclimatic changes, including sub-tropical monsoons, into the SH pattern on the millennial to sub-centennial timescales. Hence our cave record captures global signals on the millennial to sub-centennial timescales, given that Antarctic climates have wider imprints on geological archives[13,14,30].

Climate analogs and implications for ice-volume terminations. During the last glacial period, three rising limbs of the NH insolation at around 15, 39, and 60 ka BP[56] correspond to T1, MIS4/3t and HS4/DO8t, respectively. Previously, a climate sequence similar to that of the T1 is observed at MIS4/3t[27,28]. Regardless of different changing amplitudes in orbital configurations (including ice volume and insolation, Table S2), we find similar climatic fluctuations and feedbacks in the glacial-interglacial transition (T1), the sub-glacial and sub-interglacial transition (MIS4/3t) and millennial-scale sequence (HS4/DO8t) (Fig. 4 and Table S2). Bipolar temperature changes were all anti-correlated and phase-locked on the millennial timescale in the Stadial-Interstadial-Stadial sequences (Fig. 4c, h). Monsoonal records also show a strong resemblance of the millennial sequence during the HS4/DO8t and the MIS4/3t to the HS1, Bølling-Allerød and Younger Dryas events in the T1, and the sub-millennial oscillations superimposed on the three Interstadials (Fig. 4a). These are supported by atmospheric CH_4 changes which are mechanistically-related with low-latitude hydroclimate[17,57] (Fig. 4d). After removing temperature- and seawater-related deviations, we find nearly-similar millennial-scale $\delta^{18}O_{calcite}$ amplitudes across T1 (3.4‰), MIS4/3t (3‰) and HS4/DO8t (3.7‰) (Fig. S6 and Table S2), indicating recurrences of monsoonal variabilities in spite of the changing boundary conditions. In particular, the EASM variations during the HS4/DO8t are highly analogous to those in the T1 in terms of general trend and internal structures (Fig. 4a). For instance, the EASM intensity decreased during the early phase of HS1 and HS4, and then gradually increased during the second phase. Along with the phase transition, rapid monsoon weakening at 16.1 and 39.5 ka BP occurred within 20 years[41,58] and 25 years, respectively. The rapidity of the 25-year shift by 1‰ is supported by nearby annual layers at around 39 ka BP (Fig. S1 and Methods), as well as the 0.7‰ increase in 10 years induced from the highly-resolved Xianyun Cave record[59] (Fig. S3f). The similar feature is also found in DO8 Stadial and Younger Dryas, in terms of the internal centennial-scale oscillations and the much gradual onsets relative to their ends.

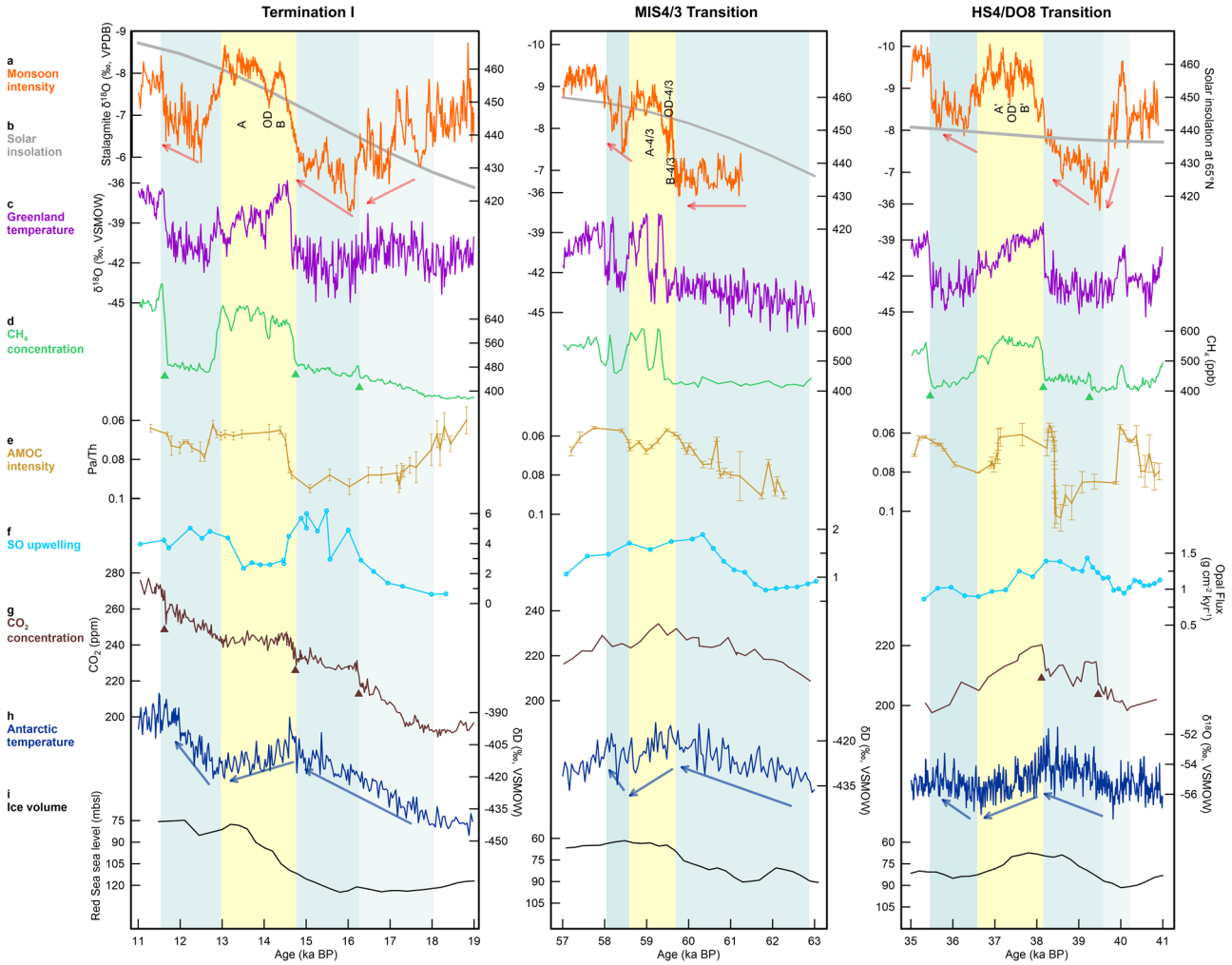

Fig. 4 Geological records across T1, the MIS4/3 transition and the HS4/DO8 transition. From top to bottom are: **a** Chinese stalagmite $\delta^{18}O_{calcite}$ records[27,29] and this study (orange), **b** solar insolation at 65°N (grey)[56], **c** NGRIP $\delta^{18}O_{ice}$ record (purple)[1], **d** atmospheric CH_4 concentrations from WDC ice core (green)[5,16], **e** Pa/Th record from the North Atlantic (gold)[62,88], **f** Opal record from Southern Ocean (blue)[63], **g** atmospheric CO_2 concentrations from ice cores in Antarctica (brown)[16,73,74], **h** Antarctic temperature record from EDC ice core (blue)[7,87] and **i** Northern Red Sea sea level record (black)[89]. Periods of millennial climatic events are denoted by colored bars. Three episodes of Bølling (B), Old Dryas (OD) and Allerød (A) within the Bølling–Allerød period are marked, and corresponding periods are coded for the MIS4/3t (middle panel) and the HS4/DO8t (right panel). Colored triangles mark centennial-scale abrupt jumps in CO_2 and CH_4. Arrows below (**a**) and (**h**) indicate changing trends of the EASM and the Antarctic temperature. The timing and duration of HS1, 4 and 6 are from ref. [90] and references therein. HS1 and HS4 include two bars, indicating periods of initial meltwater pre-events from the European ice sheet (light gray bar, early HSs) and final NH ice sheet collapse (gray bar, late HSs), respectively[66,67].

Analogous millennial-scale variations in trend, amplitude and internal centennial-scale structures of the monsoonal activities indicate the same mechanism operating throughout, which are likely related to behaviors of the ice sheet and the oscillator mode of the AMOC. During the insolation rise, extensive ice sheet collapsed (Fig. 4i) due to its inner instability or changes in the ocean subsurface temperature[60,61], leading to the stagnation of the AMOC as indicated by low Pa/Th values[62] (Fig. 4e). This causes a southward movement in ITCZ, NH monsoonal weakening (Fig. 4a) and an intensification of the upwelling[63] around the Antarctica (Fig. 4f), accounting for the CO_2 release from the Southern Ocean. However, NH monsoon intensified and the EASM-related rainfall increased upon the recovery of the AMOC, possibly due to the Agulhas salt leakage[64] or changes in the Atlantic salinity[65]. Meanwhile, opal flux was reduced and atmospheric CO_2 was decreased by the decelerated SO upwelling during the Interstadials (Fig. 4f, g). Furthermore, the meltwater pulse from the European ice sheet during the early portion of HSs and the subsequent NH ice sheet collapse during the late portion of HSs[66,67], which contributed to a much weaker AMOC during the second phase of HSs than during the early phase (Fig. 4e), could have caused the similarly twofold monsoonal phases and humidity changes during the HS1[41] and HS4 (Fig. 2). Our comparison in Figs. 3 and 4 show similar climate sequences during the last glacial period and the last deglaciation, indicating that climatic self-similarity is also applicable for glacial climate changes on different timescales (Fig. 4). Strong coupling of the climate system helps to disentangle the complex mechanism for the ice-age terminations.

Over the past decade, millennial-scale climate oscillations have been proposed to provide additional forcing to promote deglaciation by supplementing the astronomical forcing[18,19,23–25]. One recent study even addresses that millennial feedbacks in the atmosphere/ocean control the timing, structure and evolution of glacial terminations[20]. We agree with the view that the bipolar seesaw mechanism[6] responsible for the changes between Interstadials and Stadials also operated across the termination[19,23]. This mechanism exerts strong influence on the EASM, with weak

AMOC status causing decreased fraction of summer monsoon rainfall in the East Asia, decreased amount of rainout from sources to cave sites and less moisture transport to the high latitudes. According to calculations of $\delta^{18}O_{calcite}$ values by Rayleigh equation[41,68] and assumptions similar to those in Fig. S6, the remaining fractions of the original oceanic water vapor were 51% during HS1 and 42% during the Bølling period for Hulu site, 56% during HS4 and 39% during DO8 for Yongxing site, 49% during HS6 and 37% during DO17 for Wulu Cave, respectively. These results indicate that rainfall from the tropical ocean to the cave sites are relatively lower by ~20% during HSs than DO warm phases. Hence, as revealed by Chinese speleothem $\delta^{18}O$ records, the millennial-scale component might only contribute to T1 by ~60%, indicating that mechanisms other than bipolar seesaw might operate. Generally, the theory of bipolar seesaw mechanism focuses on two aspects of the ocean's role in the climate system, including the transport of heat in the Atlantic Ocean and the storage of heat in the deep ocean[6], and the transitions between different overturning states occur over a multi-centennial timescale[69]. However, this theory could only explain the smooth transitions in climates related with the oceanic processes, but could not answer the abrupt changes on the sub-centennial timescales. CO_2 and its positive feedbacks are extremely important in amplifying the initial warming during terminations[18,19,70]. Large short-term oscillations of CO_2 could enable tipping points to be reached rapidly, causing severe changes in steady-state climate[70]. Previous studies find that three remarkable CO_2 jumps contributed to more than 50% of the entire CO_2 rise (80 ppm) during the last deglaciation[16], and suggest the potential role of the AMOC, terrestrial carbon reservoir, continental shelf flooding in influencing these sudden changes[15,16,71,72]. Here, we suggest that movements of ITCZ, changes in monsoon intensity and continental components could also contribute.

During T1 and HS4/DO8t, several sub-centennial abrupt CO_2 increases with amplitudes over 10 ppm occurred around 11.6, 14.7, 16.2, 38.2, and 39.5 ka BP (Fig. 4g, triangles), although they have different amplitudes in various ice cores[35,72,73]. Two CO_2 shifts at 16.2 and 39.5 ka BP were consistent with the decadal monsoon weakening, and left no imprint in the Antarctic temperature or the AMOC records (Figs. 2 and 4). The synchronicity of the 25-year monsoonal deterioration, the 43-year and 60-ppmv CH_4 overshoot, and the abrupt CO_2 jump within 60 years in Byrd, Siple Dome and WDC ice cores[73,74] around 39.5 ka BP (Fig. 2c, e, f) implies a fast atmospheric circulation reorganization on the decadal timescale, including monsoon rainfall decrease in $\delta^{18}O_{calcite}$ by 1‰, a southward movement of the ITCZ and a strengthening of the SH westerly jet[46,74]. Analogous relationship is also found during HS1 around 16.2 ka[58]. Global model results show that the strengthening of SH westerlies could induce a multi-decadal CO_2 outgassing from the Southern Ocean, as suppressed by the southerly ITCZ and the weakened Hadley Cell[75,76]. Variations in continental ice volume and vegetation could also be the possible agents for these two multidecadal-scale CO_2 shifts. As the large reservoir of carbon, forests store 90% of the total carbon in terrestrial ecosystems[77] and a substantial global terrestrial carbon sink would slow the rate of CO_2 increase and thus climate change[78]. Thirty-one percent of Earth's total forest area is found in Asia[77] and thus influenced by the Asian Monsoon. The vegetation degradation during the HSs, especially due to centennial rapid NH ice sheet collapses[41] and the deteriorated monsoon conditions, could have hampered the CO_2 uptake by photosynthesis. Instead, the other three rapid CO_2 jumps were connected to monsoon intensification with increased rainfall, the abrupt warming in the NH and increases in CH_4 (Fig. 4). The abrupt warming in the NH was suggested to lead to massive permafrost thawing, activating a long-term immobile carbon reservoir[72]. But a recent study shows that climate wetting reduces permafrost thermal responses to warming, which is especially evident in the arid and semi-arid zones[79]. Therefore, the role of permafrost thawing still needs to be verified and the monsoon circulation needs to be considered. In short, while the AMOC shutdown leads to the millennial-scale CO_2 outgassing during the HSs, climatic components on the continent, including ice sheets, monsoon rainfall and forests, induce multi-decadal atmospheric CO_2 changes which should not be neglected when considering the causes for ice-volume terminations and future simulation work could help in testing their roles.

Methods

^{230}Th dating. Yongxing Cave is ownerless and not located within a protected nature reserve, and no federal or municipal permissions were required for collection. Sample YX175 was found broken in the cave at collection. It has a length of 165 mm, and was halved along the growth axis and polished before measurements. Nine powder subsamples (each ~100 mg) were obtained by drilling on the polished section along the growth axis with a carbide dental burr for ^{230}Th dating. ^{230}Th dating work was performed at the Isotope Laboratory, Xi'an Jiaotong University. We followed chemistry procedures to separate U and Th for dating[80]. An isotope-dilution method using in-house ^{229}Th–^{233}U–^{236}U spike was employed to determine U–Th isotopic ratios and concentrations. Nine sets of U and Th solutions were analyzed on a multi-collector inductively coupled plasma mass spectrometry (MC-ICP-MS) (Neptune-plus; Thermo-Finnigan) with an Aridus II desolvating nebulizer. Ion beams were measured in peak-jumping mode on the secondary electron multiplier behind the retarding potential quadrupole and followed similar procedures as described in previous study[81]. The instrumentation, standardization, and half-lives were reported[82,83]. Uncertainties in U–Th isotopic data were calculated at the 2σ level, including corrections for blanks, multiplier darknoise, abundance sensitivity, and contents of the same nuclides in the spike solution. Corrected ^{230}Th ages assume an initial ^{230}Th/^{232}Th atomic ratio of $4.4 \pm 2.2 \times 10^{-6}$ and the values for a material at secular equilibrium with the bulk earth ^{232}Th/^{238}U value of 3.8. Most samples have high ^{230}Th/^{232}Th ratios and thus minor corrections. These ^{230}Th dates have typical age uncertainties of less than 112 years (Table S1), all in stratigraphic order.

Oxygen isotope analysis. Subsamples (each ~50 μg) for stable isotope analysis were shaved at a resolution of 0.1 mm from along the central growth axis with a knife. Every second subsample ($n = 826$) was measured, using a Finnigan-MAT 253 mass spectrometer fitted with a Kiel Carbonate Device at the School of Geography, Nanjing Normal University, China. CO_2 was released from the carbonate by reaction under vacuum with 105% H_3PO_4 at 90 °C. Each gaseous sample was scanned six times, and calibrated against a reference CO_2 gas. All results are reported in parts per mil (‰) relative to the Vienna Pee Dee Belemnite (VPDB) standard and have 0.06‰ at the 1σ level. Repeated analyses of an international standard (NBS19; $\delta^{18}O = -2.20$‰; VPDB) between every 10 subsamples was used to check the long-term reproducibility.

Chronology and annual layer counting. An age model was then developed using Oxcal Project due to its better fitting with ^{230}Th dates and the estimated errors[84,85] (Fig. S1), yielding a time range from 40.89 to 33.08 ka BP (present = 1950 AD). The average temporal resolution reaches approximately 10 years. Furthermore, between 81 mm and 82 mm depth and 130 mm and 131 mm depth of our sample, 52 ± 5 and 55 ± 3 of couplets of light/dark layers can be identified per millimeter under optical microscope. If these are annual bands, they would indicate a growth rate of 1.7–2.1 mm/century (Fig. S1), which agrees reasonably well with our estimate of 18.2–19.5 mm/ka from the bounding U/Th dates (at depths of 61 mm, 86 mm, 124.5 mm and 141.5 mm).

Data availability

Stable-isotope and U-series data of our sample have been deposited in the Mendeley dataset (https://doi.org/10.17632/n82f6dskdh.1).

Received: 26 March 2022; Accepted: 16 November 2022;
Published online: 28 November 2022

References

1. Andersen, K. K. et al. High-resolution record of Northern Hemisphere climate extending into the last interglacial period. *Nature* **431**, 147–151 (2004).
2. Heinrich, H. Origin and consequences of cyclic ice rafting in the Northeast Atlantic Ocean during the past 130,000 years. *Quat. Res.* **29**, 142–152 (1988).

3. Blunier, T. & Brook, E. J. Timing of millennial-scale climate change in Antarctica and Greenland during the last glacial period. *Science* **291**, 109–112 (2001).
4. EPICA Community Members C. One-to-one coupling of glacial climate variability in Greenland and Antarctica. *Nature* **444**, 195–198 (2006).
5. WAIS Divide Project Members. Precise interpolar phasing of abrupt climate change during the last ice age. *Nature* **520**, 661–665 (2015).
6. Stocker, T. F. & Johnsen, S. J. A minimum thermodynamic model for the bipolar seesaw. *Paleoceanography* **18**, 1087 (2003).
7. Landais, A. et al. A review of the bipolar see–saw from synchronized and high resolution ice core water stable isotope records from Greenland and East Antarctica. *Quat. Sci. Rev.* **114**, 18–32 (2015).
8. Braun, H. et al. Possible solar origin of the 1470-year glacial climate cycle demonstrated in a coupled model. *Nature* **438**, 208–211 (2005).
9. Baldini, J. U. L. et al. Was millennial scale climate change during the Last Glacial triggered by explosive volcanism? *Sci. Rep.* **5**, 17442 (2015).
10. Pedro, J. B. et al. Beyond the bipolar seesaw: toward a process understanding of interhemispheric coupling. *Quat. Sci. Rev.* **192**, 27–46 (2018).
11. Buizert, C. et al. Abrupt ice-age shifts in southern westerly winds and Antarctic climate forced from the north. *Nature* **563**, 681–685 (2018).
12. Capron, E. et al. Millennial and sub-millennial scale climatic variations recorded in polar ice cores over the last glacial period. *Clim. Past* **6**, 345–365 (2010).
13. Thirumalai, K., Clemens, S. C. & Partin, J. W. Methane, monsoons, and modulation of millennial-scale climate. *Geophys. Res. Lett.* **47**, e2020GL087613 (2020).
14. Barker, S. & Knorr, G. Antarctic climate signature in the Greenland ice core record. *Proc. Natl. Acad. Sci. Unit. States Am.* **104**, 17278–17282 (2007).
15. Chen, T. et al. Synchronous centennial abrupt events in the ocean and atmosphere during the last deglaciation. *Science* **349**, 1537–1541 (2015).
16. Marcott, S. A. et al. Centennial-scale changes in the global carbon cycle during the last deglaciation. *Nature* **514**, 616–619 (2014).
17. Rhodes, R. H. et al. Enhanced tropical methane production in response to iceberg discharge in the North Atlantic. *Science* **348**, 1016–1019 (2015).
18. Cheng, H. et al. The Asian monsoon over the past 640,000 years and ice age terminations. *Nature* **534**, 640–646 (2016).
19. Denton, G. H. et al. The last glacial termination. *Science* **328**, 1652–1656 (2010).
20. Barker, S. Millennial scale feedbacks determine the shape and rapidity of glacial termination. *Nat. Commun.* **12**, 2273 (2021).
21. Wang, Y. et al. Millennial- and orbital- scale changes in the East Asian Monsoon over the past 224,000 years. *Nature* **451**, 1090–1093 (2008).
22. Margari, V. et al. The nature of millennial-scale climate variability during the past two glacial periods. *Nat. Geosci.* **3**, 127–131 (2010).
23. Cheng, H. et al. Ice age terminations. *Science* **326**, 248–252 (2009).
24. Wolff, E. W., Fischer, H. & Röthlisberger, R. Glacial terminations as southern warmings without northern control. *Nat. Geosci.* **2**, 206–209 (2009).
25. Barker, S., Knorr, G., Vautravers, M. J., Diz, P. & Skinner, L. Extreme deepening of the Atlantic overturning circulation during deglaciation. *Nat. Geosci.* **3**, 567–571 (2010).
26. Vázquez Riveiros, N. et al. The "MIS 11 paradox" and ocean circulation: Role of millennial scale events. *Earth Planet. Sci. Lett.* **371**, 258–268 (2013).
27. Liu, D. et al. Sub-millennial variability of Asian monsoon intensity during the early MIS 3 and its analogue to the ice age terminations. *Quat. Sci. Rev.* **29**, 1107–1115 (2010).
28. Schaefer, J. M. et al. The Southern Glacial Maximum 65,000 years ago and its Unfinished Termination. *Quat. Sci. Rev.* **114**, 52–60 (2015).
29. Wang, Y. et al. A high-resolution absolute-dated late Pleistocene monsoon record from Hulu Cave, China. *Science* **294**, 2345–2348 (2001).
30. Chen, S. et al. Strong coupling of Asian Monsoon and Antarctic climates on sub-orbital timescales. *Sci. Rep.* **6**, 32995 (2016).
31. Thirumalai, K. et al. Methane, monsoons, and modulation of millennial-scale climate. *Geophys. Res. Lett.* **47**, e2020GL087613 (2020).
32. Rohling, E. et al. Controls on the East Asian monsoon during the last glacial cycle, based on comparison between Hulu Cave and polar ice-core records. *Quat. Sci. Rev.* **28**, 3291–3302 (2009).
33. Wang, Z. et al. Sixty-year quasi-period of the Asian monsoon around the Last Interglacial derived from an annually resolved stalagmite δ18O record. *Palaeogeogr., Palaeoclimatol., Palaeoecol.* **541**, 109545 (2020).
34. Zhao, X. et al. A high-resolution speleothem record of Marine Isotope Stage 11 as a natural analog to Holocene Asian summer monsoon variations. *Geophys. Res. Lett.* **46**, 9949–9957 (2019).
35. Dorale, J. A. & Liu, Z. Limitations of Hendy test criteria in judging the paleoclimatic suitability of speleothems and the need for replication. *J. Cave Karst Stud.* **71**, 73–80 (2009).
36. Wang, Q. et al. The transfer of oxygen isotopic signals from precipitation to drip water and modern calcite on the seasonal time scale in Yongxing Cave, central China. Environ. *Earth Sci.* **77**, 1–18 (2018).
37. Zhao, K. et al. East Asian monsoon changes and its ENSO response revealed by a 200-year stalagmite record from Yongxing Cave on the Mountain Shengnongjia. *Geogr. Res.* **34**, 74–84 (2015). (in Chinese).
38. Tong, J. et al. Yangtze floods and droughts (China) and teleconnections with ENSO activities (1470–2003). *Quat. Int.* **144**, 29–37 (2006).
39. Zhao, G. J. et al. A new upper-level circulation index for the East Asian summer monsoon variability. *J. Clim.* **28**, 99779–99996 (2015).
40. Wang, M. et al. Stalagmite multi-proxy evidence of wet and dry intervals in the middle Yangtze Valley during the last glacial period. *Palaeogeogr. Palaeoclimatol. Palaeoecol.* **586**, 110764 (2021).
41. Liang, Y. et al. East Asian monsoon changes early in the last deglaciation and insights into the interpretation of oxygen isotope changes in the Chinese stalagmite record. *Quat. Sci. Rev.* **250**, 106699 (2020).
42. Mudelsee, M. Ramp function regression: a tool for quantifying climate transitions. *Comput. Geosci.* **26**, 293–307 (2000).
43. Bock, M. et al. Hydrogen isotopes preclude marine hydrate CH4 Emissions at the onset of Dansgaard-Oeschger events. *Science* **328**, 1686–1689 (2010).
44. Erhardt, T. et al. Decadal-scale progression of the onset of Dansgaard–Oeschger warming events. *Clim. Past* **15**, 811–825 (2019).
45. Guillevic, M. et al. Evidence for a three-phase sequence during Heinrich Stadial 4 using a multiproxy approach based on Greenland ice core records. *Clim. Past* **10**, 2115–2133 (2014).
46. Gadgil, S. The monsoon system: Land–sea breeze or the ITCZ? *J. Earth Syst. Sci.* **127**, 1–29 (2018).
47. Schneider, T., Bischoff, T. & Haug, G. H. Migrations and dynamics of the intertropical convergence zone. *Nature* **513**, 45–53 (2014).
48. Chiang, J. C. H., Lee, S., Putnam, A. E. & Wang, X. South Pacific Split Jet, ITCZ shifts, and atmospheric North–South linkages during abrupt climate changes of the last glacial period. *Earth Planet. Sci. Lett.* **406**, 233–246 (2014).
49. McGee, D., Donohoe, A., Marshall, J. & Ferreira, D. Changes in ITCZ location and cross-equatorial heat transport at the Last Glacial Maximum, Heinrich Stadial 1, and the mid-Holocene. *Earth Planet. Sci. Lett.* **390**, 69–79 (2014).
50. Hawcroft, M. et al. Southern Ocean albedo, inter-hemispheric energy transports and the double ITCZ: global impacts of biases in a coupled model. *Clim. Dynam.* **48**, 2279–2295 (2016).
51. Buizert, C. et al. The WAIS Divide deep ice core WD2014 chronology – Part 1: Methane synchronization (68–31 ka BP) and the gas age–ice age difference. *Clim. Past* **11**, 153–173 (2014).
52. Clemens, S. C., Murray, D. W. & Prell, W. L. Nonstationary phase of the Plio-Pleistocene Asian Monsoon. *Science* **274**, 943–948 (1996).
53. Xue, F., Wang, H. & He, J. Interannual variability of Mascarene High and Australian High and their influences on East Asian summer monsoon. *J. Meteorol. Soc. Japan* **82**, 1173–1186 (2004).
54. Nan, S., Li, J., Yuan, X. & Zhao, P. Boreal spring Southern Hemisphere Annular Mode, Indian Ocean sea surface temperature, and East Asian. *summer monsoon. J. Geophys. Res.* **114**, D02103 (2009).
55. Davis, W. J., Taylor, P. J. & Davis, W. B. The origin and propagation of the antarctic centennial oscillation. *Climate* **7**, 112 (2019).
56. Berger, A. Long-term variations of caloric insolation resulting from the Earth's orbital elements. *Quat. Res.* **9**, 139–167 (1978).
57. Guo, Z., Zhou, X. & Wu, H. Glacial-interglacial water cycle, global monsoon and atmospheric methane changes. *Clim. Dynam.* **39**, 1073–1092 (2011).
58. Zhang, W. et al. A detailed East Asian monsoon history surrounding the 'Mystery Interval' derived from three Chinese speleothem records. *Quat. Res.* **82**, 154–163 (2014).
59. Zhang, X. et al. Three-phase structure of the East Asia summer monsoon during Heinrich Stadial 4 recorded in Xianyun Cave, southeastern China. *Quat. Sci. Rev.* **274**, 107267 (2021).
60. MacAyeal, D. R. Binge/purge oscillations of the Laurentide Ice Sheet as a cause of the North Atlantic's Heinrich events. *Paleoceanography* **8**, 775–784 (1993).
61. Bassis, J. N., Petersen, S. V. & Cathles, L. M. Heinrich events triggered by ocean forcing and modulated by isostatic adjustment. *Nature* **542**, 332–334 (2017).
62. Henry, L. G. et al. North Atlantic Ocean circulation and abrupt climate change during the last glaciation. *Science* **353**, 470–474 (2016).
63. Anderson, R. F. et al. Wind-driven upwelling in the Southern Ocean and the deglacial rise in atmospheric CO_2. *Science* **323**, 1443–1448 (2009).
64. Simon, M. H. et al. Millennial-scale Agulhas Current variability and its implications for salt-leakage through the Indian–Atlantic Ocean Gateway. *Earth Planet. Sci. Lett.* **383**, 101–112 (2013).
65. Ackermann, L., Danek, C., Gierz, P. & Lohmann, G. AMOC Recovery in a multicentennial scenario using a coupled atmosphere-ocean-ice sheet model. *Geophys. Res. Lett.* **47**, e2019GL086810 (2020).
66. Toucanne, S. et al. Millennial-scale fluctuations of the European Ice Sheet at the end of the last glacial, and their potential impact on global climate. *Quat. Sci. Rev.* **123**, 113–133 (2015).
67. Plaza-Morlote, M. et al. Southernmost evidence of large European Ice Sheet-derived freshwater discharges during the Heinrich Stadials of the Last Glacial

Period (Galician Interior Basin, Northwest Iberian Continental Margin). *Earth Planet. Sci. Lett.* **457**, 213–226 (2017).
68. Yuan, D. et al. Timing, Duration, and Transitions of the Last Interglacial Asian Monsoon. *Science* **304**, 575–578 (2004).
69. Thompson, A. F., Hines, S. K. & Adkins, J. F. A Southern Ocean mechanism for the interhemispheric coupling and phasing of the bipolar seesaw. *J. Clim.* **32**, 4347–4365 (2019).
70. Steinthorsdottir, M., Wohlfarth, B., Kylander, M. E., Blaauw, M. & Reimer, P. J. Stomatal proxy record of CO_2 concentrations from the last termination suggests an important role for CO_2 at climate change transitions. *Quat. Sci. Rev.* **68**, 43–58 (2013).
71. Köhler, P. et al. Abrupt rise in atmospheric CO_2 at the onset of the Bølling/Allerød: in-situ ice core data versus true atmospheric signals. *Clim. Past* **7**, 473–486 (2011).
72. Köhler, P., Knorr, G. & Bard, E. Permafrost thawing as a possible source of abrupt carbon release at the onset of the Bølling/Allerød. *Nat. Commun.* **5**, 5520 (2014).
73. Bauska, T. K., Marcott, S. A. & Brook, E. J. Abrupt changes in the global carbon cycle during the last glacial period. *Nat. Geosci.* **14**, 91–96 (2021).
74. Ahn, J., Brook, E. J., Schmittner, A. & Kreutz, K. Abrupt change in atmospheric CO2 during the last ice age. *Geophys. Res. Lett.* **39**, L18711 (2012).
75. Lee, S., Chiang, J. C., Matsumoto, K. & Tokos, K. Southern Ocean wind response to North Atlantic cooling and the rise in atmospheric CO_2: Modeling perspective and paleoceanographic implications. *Paleoceanography* **26**, PA1214 (2011).
76. Menviel, L. C. et al. Southern Hemisphere westerlies as a driver of the early deglacial atmospheric CO_2 rise. *Nat. Commun.* **9**, 2503 (2018).
77. Pan, Y., Birdsey, R., Phillips, O. L. & Jackson, R. B. The structure, distribution, and biomass of the World's forests. *Annu. Rev. Ecol. Evol. Syst.* **44**, 593–622 (2013).
78. Walker, A. P. et al. Integrating the evidence for a terrestrial carbon sink caused by increasing atmospheric CO_2. *New phytol.* **229**, 2413–2445 (2020).
79. Zhang, G., Nan, Z., Zhao, L., Liang, Y. & Cheng, G. Qinghai-Tibet Plateau wetting reduces permafrost thermal responses to climate warming. *Earth Planet. Sci. Lett.* **562**, 116858 (2021).
80. Edwards, L. R., Chen, J. H. & Wasserburg, G. J. ^{238}U-^{234}U-^{230}Th-^{232}Th systematics and the precise measurement of time over the past 500,000 years. *Earth Planet. Sci. Lett.* **81**, 175–192 (1987).
81. Shen, C.-C. et al. High-precision and high-resolution carbonate ^{230}Th dating by MC-ICP-MS with SEM protocols. *Geochim. Cosmochim. Acta* **99**, 71–86 (2012).
82. Cheng, H. et al. Improvements in ^{230}Th dating, ^{230}Th and ^{234}U half-life values, and U–Th isotopic measurements by multi-collector inductively coupled plasma mass spectrometry. *Earth Planet. Sci. Lett.* **371–372**, 82–91 (2013).
83. Jaffey, A. H., Flynn, K. F., Glendenin, L. E., Bentley, W. C. & Essling, A. M. Precision measurement of half-lives and specific activities of ^{235}U and ^{238}U. *Phys. Rev. C* **4**, 1889–1906 (1971).
84. Ramsey, C. & Lee, S. Recent and planned developments of the program OxCal. *Radiocarbon* **55**, 720–730 (2013).
85. Ramsey, C. Deposition models for chronological records. *Quat. Sci. Rev.* **27**, 42–60 (2008).
86. Svensson, A. et al. A 60,000 year Greenland stratigraphic ice core chronology. *Clim. Past* **3**, 47–57 (2008).
87. Veres, D. et al. The Antarctic ice core chronology (AICC2012): An optimized multi-parameter and multi-site dating approach for the last 120 thousand years. *Clim. Past* **9**, 1733–1748 (2013).
88. McManus, J. F., Francois, R., Gherardi, J.-M., Keigwin, L. D., & Brown-Leger, S. Collapse and rapid resumption of Atlantic meridional circulation linked to deglacial climate changes. *Nature* **428**, 834–837 (2004).
89. Arz, H. W., Lamy, F., Ganopolski, A., Nowaczyk, N. & Pätzold, J. Dominant Northern Hemisphere climate control over millennial-scale glacial sea-level variability. *Quat. Sci. Rev.* **26**, 312–321 (2007).
90. Seierstad, K. et al. Consistently dated records from the Greenland GRIP, GISP2 and NGRIP ice cores for the past 104 ka reveal regional millennial-scale $\delta^{18}O$ gradients with possible Heinrich event imprint. *Quat. Sci. Rev.* **106**, 29–46 (2014).

Acknowledgements

We would like to thank Dr. A. Landais for sharing the EDC and TALDICE ice core $\delta^{18}O$ data. This work was funded by the National Research Foundation of China (award no. 42072207 to S.C., 41931178 to Y.W., no. 42071105 to K.Z.), Jiangsu Center for Collaborative Innovation in Geographical Information Resource Development and Application, the U.S. National Science Foundation (award no. 1702816 to R.L.E.), the 111 Program of China (award no. D19002 to R.L.E.) and the State Key Laboratory of Loess and Quaternary Geology, Institute of Earth Environment, CAS (award no. SKLLQG2120 to Y.L).

Author contributions

Y.L. carried out the uranium/thorium dating and oxygen isotope measurements, counted the lamina on sliced-samples and wrote the manuscript. S.C. designed the project, performed the fieldwork and sampling and wrote the manuscript. Y.W. designed the project and wrote the manuscript. K.Z. performed the fieldwork and sampling. S.Y. performed the fieldwork and sampling. Z.W. counted the lamina on sliced-samples and oxygen isotope measurements. Y.H. performed the fieldwork and sampling, carried out the uranium/thorium dating and oxygen isotope measurements. H.C. carried out the uranium/thorium dating. R.L.W. carried out the uranium/thorium dating. All the authors discussed the results and implications and commented on the manuscript. We also thank the editors and two reviewers very much for their insightful comments and suggestions that helped a lot in improving this paper.

Competing interests

The authors declare no competing interests.

Additional information

Supplementary information The online version contains supplementary material available at https://doi.org/10.1038/s43247-022-00633-0.

Correspondence and requests for materials should be addressed to Shi-Tao Chen.

Peer review information *Communications Earth & Environment* thanks the anonymous reviewers for their contribution to the peer review of this work. Primary Handling Editors: Olga Churakova, Joe Aslin. Peer reviewer reports are available.

Reprints and permission information is available at http://www.nature.com/reprints

Publisher's note Springer Nature remains neutral with regard to jurisdictional claims in published maps and institutional affiliations.